

Non-monotonic spin-phase gathering in curved spintronic circuits

Eusebio J. Rodríguez and Diego Frustaglia*

Departamento de Física Aplicada II, Universidad de Sevilla, E-41012 Sevilla, Spain

(Dated: September 3, 2022)

Spin carriers in a two-dimensional electron gas can be manipulated by introducing spin-orbit coupling (SOC) and geometric constraints. By working with one-dimensional models, we show that spin carriers propagating in circuits of polygonal shape gather spin phases in a non-monotonic fashion as a function of the Rashba SOC strength. The complex interplay between dynamic and geometric spin-phase components leads to bounded, global spin phases. This peculiar behaviour is triggered by the inhomogeneities of the geometric curvature along the polygonal perimeter—where flat segments alternate with highly curved vertices—introducing effective Rashba field discontinuities acting as scattering centers for spin. As a consequence, a periodic series of spin degeneracy points emerge. This contrasts with the case of wires and rings (circuits of constant curvature) presenting a monotonous spin-phase gathering. We show that the particulars of the spin-phase gathering have observable consequences in the Aharonov-Casher conductance of Rashba loops. Our findings offer original ways to engineer electronic spin phases at the mesoscopic scale by geometric means.

I. INTRODUCTION

Spin dynamics can be determinant for electronic transport in mesoscopic conductors.¹ Carriers developing spin-dependent phases experience quantum interference effects molding properties such as the conductance. Coherent spin-phase contributions can be so strong that they even reverse the magnetoconductance response of low-dimensional systems, as in the case of weak (anti)localization.^{2,3} A prominent source of spin phases in two-dimensional electron gases is spin-orbit coupling (SOC), responsible for the working principles of spin-field-effect transistors^{4–7} and Aharonov-Casher (AC) interferometers,^{8–14} among others.^{15,16} Moreover, when SOC is combined with Zeeman fields and superconducting proximity effects, spin carriers can develop more exotic quantum states of topological nature such as the celebrated (and elusive) Majorana modes.¹⁷

The electrical modulation of the Rashba SOC¹⁸ in two-dimensional electron gases¹⁹ has facilitated the realization of spin interferometers^{12–14} based on the AC effect.⁸ This is an electrical effect on a particle carrying a quantum magnetic moment, which is nothing but the electromagnetic dual of the Aharonov-Bohm (AB) effect²⁰ (a magnetic effect on an electrically charged quantum particle). The role played by dynamic and geometric spin phases in the conductance of AC interferometers (specially in mesoscopic rings) has been studied intensively over the last decade.^{21–25} Moreover, further studies on polygonal AC interferometers^{26–29} have demonstrated that the conductance is quite sensitive to the geometric shape of the conducting channels (specifically, to their curvature^{30–32,34}) due to the development of strongly non-adiabatic spin dynamics.³⁵ This has significant consequences on the response to external fields and the generation of topological spin phases.³³ Still, some questions remain open in this regard as the interplay between dynamic and geometric spin-phase gathering and their distinct contributions.

Here, we address these questions by studying the development of dynamic and geometric phases in spin carriers propagating through one-dimensional model loops of polygonal shape subject to Rashba SOC. By these means, we find that the spin-phase gathering in Rashba polygons is strongly non-monotonic, in manifest contrast to what observed in Rashba rings. Our results show that this is a direct consequence of spin degeneracies emerging from the non-adiabatic spin dynamics triggered by field discontinuities at the polygon vertices. These features lead to a series of remarkable effects such as, e.g., the upper bounding of global spin phases, the possibility of purely geometric spin-phase gathering (due to vanishing dynamic spin phases), and the development of geometric spin-phase plateaus that allow the independent control of dynamic spin phases (complementary to previous findings regarding the independent control of geometric spin phases in rings²²).

We point out that one-dimensional models for spin-carrier transport in mesoscopic interferometers have been used in the past with success.^{11,22,26,29,33,36–38} In particular, models similar to the one employed here have demonstrated to be well suited to experiments with arrays of interferometric loops where only one single (quasi-one-dimensional) orbital mode appears to contribute to quantum interference due to the decoherence experienced by relatively slow propagating higher modes.^{22,33}

The paper is organized as follows. In Sec. II we introduce a one-dimensional model for conducting Rashba polygons. Our results on non-monotonic spin-phase gathering are presented in Sec. III A. In Sec. III B we discuss the consequences of the spin-phase gathering process in the conductance of Rashba loops. Sec. IV is devoted to closing comments and conclusions. Some details on a semiclassical approach to the quantum conductance of Rashba loops are presented in an appendix.

II. MODEL

Consider a regular polygon of perimeter P lying on the xy -plane consisting of N conducting segments of length $L = P/N$ connecting vertices u and v and oriented along directions $\hat{\gamma}_{vu}$ (from u to v), see Fig. 1. The spin-carrier dynamics along each wire segment is determined by the Hamiltonian²⁶

$$H_{vu} = \frac{p_\ell^2}{2m} + \frac{\alpha_R}{\hbar} p_\ell (\hat{\gamma}_{vu} \times \hat{\mathbf{z}}) \cdot \boldsymbol{\sigma} \quad (1)$$

with $p_\ell = -i\hbar\partial_\ell$ the linear momentum of the spin-carriers, ℓ the linear coordinate along the wire, and α_R the Rashba SOC strength (which can be controlled in experiments by electrical means¹⁹). The second term in Eq. (1) represents an effective in-plane magnetic field $\mathbf{B}_R = (2\alpha_R/\hbar g \mu_B) p_\ell (\hat{\gamma}_{vu} \times \hat{\mathbf{z}})$ coupled to the itinerant spins, with g the g -factor and μ_B the Bohr magneton. Notice that \mathbf{B}_R is normal to $\hat{\gamma}_{vu}$, inverting its sign for counterpropagating carriers. This means that H_{vu} preserves time-reversal symmetry. Spin carriers propagating around polygonal loops undergo a series of effective-field discontinuities at the vertices due to the abrupt changes of $\hat{\gamma}_{vu}$, with significant consequences for the spin dynamics. Ring-shaped loops can be modelled as polygons by taking the limit $N \gg 1$ while keeping P constant. In this limit, a radial \mathbf{B}_R emerges and the field discontinuities disappear.²⁶ Moreover, the Rashba SOC strength can be expressed in terms of the phase $k_R P$ gathered by a spin carrier propagating along a segment of length P , with $k_R = \alpha_R m/\hbar^2 = \pi/L_R$ and L_R the spin-precession length.

By completing squares in Eq. (1), we find that the propagation of a spin carrier from u to v is fully determined by the phases $k_F L + k_R L (\hat{\gamma}_{vu} \times \hat{\mathbf{z}}) \cdot \boldsymbol{\sigma}$, with k_F the Fermi wavenumber. In particular, we notice that the spin evolution along the segment is given by the momentum-independent spin rotation operator

$$R_{vu} = \exp[-ik_R L (\hat{\gamma}_{vu} \times \hat{\mathbf{z}}) \cdot \boldsymbol{\sigma}], \quad (2)$$

with $R_{vu}^\dagger = R_{uv}$ due to time-reversal symmetry. Equation (2) is the building block to describe the spin evolution of a carrier propagating around a polygonal loop. By labelling the vertices from 1 to N , we find that spin evolution along counterclockwise (CCW) and clockwise (CW) propagating paths is given by the unitary operators

$$U_+(N) = R_{1N} \dots R_{32} R_{21}, \quad (3)$$

$$U_-(N) = R_{12} \dots R_{N-1,N} R_{N1}, \quad (4)$$

respectively, with $U_-(N) = U_+^\dagger(N)$. The eigenvalue equation

$$U_\pm(N)|\chi_s\rangle = \exp[\pm i\phi_s]|\chi_s\rangle \quad (5)$$

defines the total spin phase $\pm\phi_s$ gathered by a carrier after a CCW/CW round trip propagating from the initial

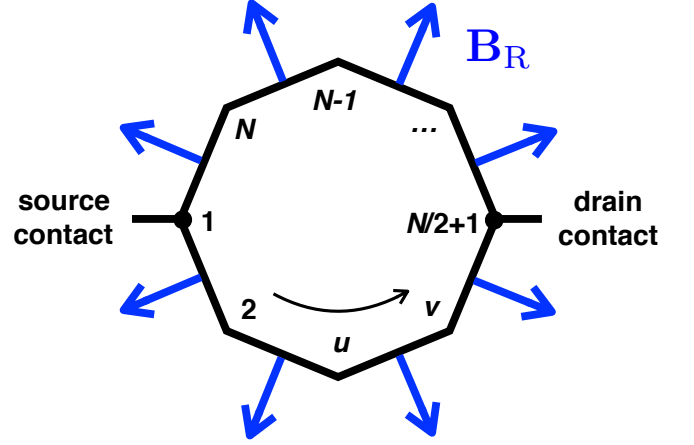


FIG. 1. One-dimensional Rashba polygon model. The effective Rashba field \mathbf{B}_R correspond to CCW propagating spin carriers.

state $|\chi_s\rangle$ to a final state $\exp[\pm i\phi_s]|\chi_s\rangle$ defined at the initial vertex 1, with $s = \uparrow, \downarrow$ and $\langle\chi_\uparrow|\chi_\downarrow\rangle = 0$. In regular polygons, symmetry dictates that the spin quantization axis $\hat{n}_s = \langle\chi_s|\boldsymbol{\sigma}|\chi_s\rangle$ is contained within the plane normal to the polygon that bisects the vertex's angle. This means that full alignment of \hat{n}_s and \mathbf{B}_R is forbidden and that the initial state $|\chi_s\rangle$ propagates along the corresponding segment by precessing around the local \mathbf{B}_R . This repeats identically for every vertex and segment. It is only in the $N \gg 1$ limit (ring-shaped loops) that the spin eigenmodes can eventually reach a full alignment with the local \mathbf{B}_R for sufficiently large Rashba-field strengths (adiabatic regime).¹¹ This is illustrated by the Bloch-sphere insets shown in Fig. 2.

The global spin phase $\phi_s = \phi_d^s + \phi_g^s$ splits into dynamic (ϕ_d^s) and geometric (ϕ_g^s) phase contributions.³⁹ The dynamic spin phase represents the expectation value of the spin Hamiltonian over the propagating spin modes in a CCW round trip. Due to symmetry, it reduces to $\phi_d^s = -k_R P (\hat{\gamma}_{21} \times \hat{\mathbf{z}}) \cdot \hat{n}_s$. The geometric spin phase $\phi_g^s = -\Omega_s/2$, instead, is proportional to the solid angle Ω_s subtended by the spin modes in the Bloch sphere after a CCW round trip is completed. The global and dynamical spin phases, ϕ_s and ϕ_d^s , are obtained easily by solving Eq. (5). An explicit calculation of the geometric spin phase ϕ_g^s is sometimes difficult, but unnecessary in our case: it can be simply obtained from the other two as their difference, $\phi_g^s = \phi_s - \phi_d^s$.

A similar analysis applies to CW propagating spin carriers by replacing ϕ_s with $-\phi_s$, as seen from Eq. (5).

III. RESULTS

We start by calculating the global (ϕ_s), dynamic (ϕ_d^s), and geometric (ϕ_g^s) spin phases gathered by carriers in polygonal loops with an even N . The results show a rich

dynamics as compared to ring-shaped loops, with several possibilities for spin-phase manipulation. We then put this features into correspondence with transport properties.

A. Spin phases

For the sake of simplicity we focus our attention on CCW propagating spin-up ($s = \uparrow$) carriers. We define the spin-up species as the branch for which $|\chi_\uparrow\rangle \rightarrow |\uparrow\rangle_z$ as the Rashba SOC vanishes ($k_R \rightarrow 0$), where $|\uparrow\rangle_z$ is the eigenstate of σ_z with positive eigenvalue. Henceforth, we drop the spin label from the global (ϕ), dynamic (ϕ_d), and geometric (ϕ_g) spin phases.

In Fig. 2 we plot the discriminated spin phases as a function of the Rashba SOC strength $k_R P$ for (a) squares, (b) hexagons, (c) octagons, and (d) rings. It stands out the strongly non-monotonic response of the spin phases in polygons, contrasting with a purely monotonic behavior in the ring's case. We observe that the global spin phase ϕ (black) for polygons is *bounded*, oscillating with a periodicity $2N\pi$ from 0 to $(N-2)\pi$. This unexpected bounding is the consequence of a singular interplay between dynamic and geometric phase components in polygons, ϕ_d (blue) and ϕ_g (red), which oscillate counterphase with an increasing amplitude.

In Figs. 2(a), 2(b) and 2(c), the oscillating dynamic spin phase ϕ_d (blue) reveals aspects of an intricate spin evolution (see the corresponding spin textures in the Bloch-sphere insets). Its sign is indicative of the spin-state projection along the local Rashba field \mathbf{B}_R (negative projection for positive ϕ_d , and viceversa). Its growing amplitude is an expected consequence of the increasing Rashba-field strength, even for partial spin-state/field alignment. The most interesting feature is the vanishing of ϕ_d at $k_R P = nN\pi$ (n integer), corresponding to spin degeneracy points. This corresponds to spinors $|\chi_s\rangle$ quantized along the z -axis, such that spins propagate along the polygons perimeter by precessing within a plane perpendicular to the local Rashba field \mathbf{B}_R . These states are illustrated in Figs. 2(a), 2(b) and 2(c) by the insets corresponding to $k_R P = 4\pi, 6\pi$, and 8π , respectively.

As for the geometric spin phase ϕ_g (red), its sign indicates the dominating orbiting direction of the spin states in the Bloch sphere while its magnitude grows with the number of orbiting loops (multiplying the subtended solid angle). Notice that a vanishing ϕ_g , except for the case of $k_R P = 0$, is not a signal of pinned spin states but, instead, an indicator of complex spin textures where loops with different orbiting directions in the Bloch sphere contribute with partial solid angles of opposite sign that cancel exactly. An example in Rashba squares, Fig. 2(a), takes place at $k_R P = 3\pi$: the corresponding spin texture is shown with further detail in Fig. 3 by including an azimuthal projection where positive and negative contributions are identified. The periodic devel-

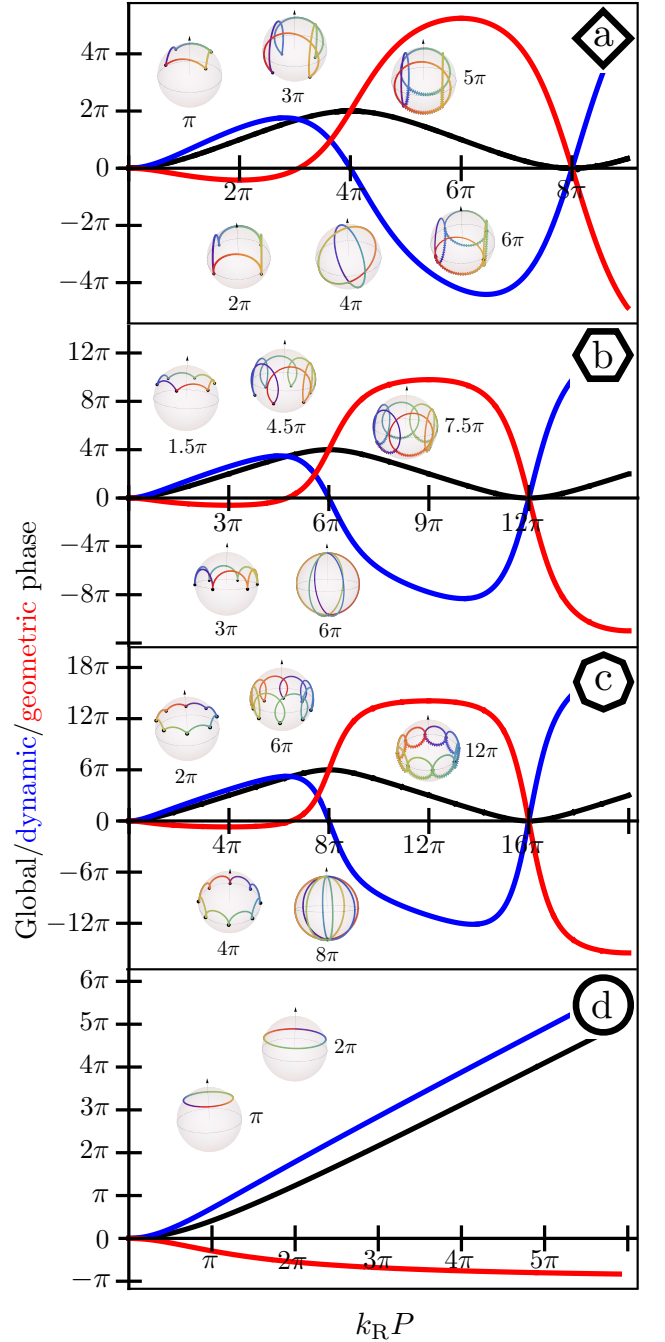


FIG. 2. Global (black), dynamic (blue) and geometric (red) phases of propagating spin modes in Rashba squares (a), hexagons (b), octagons (c), and rings (d) as a function of the Rashba SOC strength $k_R P$. The spin degeneracy points are those where the dynamic phase (blue) vanishes. The Bloch-sphere insets depict the spin textures corresponding to propagating modes for different values of $k_R P$ (the solid dots coincide with the polygons' vertices). The complex response of the spin phases and textures for polygons contrast with the monotonic response for rings.

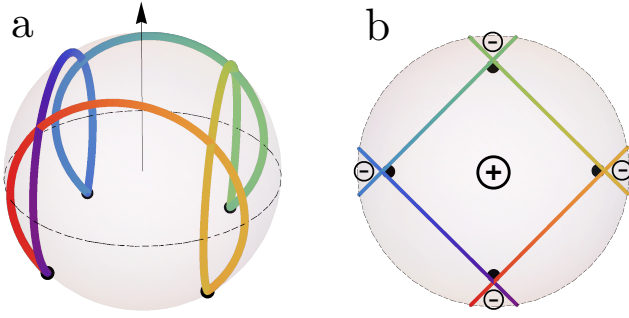


FIG. 3. (a) Bloch sphere showing the spin texture of a propagating mode with vanishing geometric phase in a Rashba square corresponding to $k_R P = 3\pi$, see Fig. 2(a). (b) Azimuthal projection indicating the positive and negative contributions to the solid angle. The solid dots coincide with the square's vertices.

opment of opposite contributions of this kind lead to the oscillating response of ϕ_g in polygons shown in Figs. 2(a), 2(b) and 2(c). Two particular features stand out here: (i) ϕ_g tends to develop plateaus in the vicinity of its extremes. This tendency is more pronounced as the number of sides N increases. Interestingly, within a geometric-phase plateau the global phase ϕ presents a linear evolution as a function of $k_R P$ with origin in the dynamic component ϕ_d . This shows the possibility of an independent control of the dynamic spin-phase component ϕ_d in Rashba polygons, complementary to the purely geometric spin phase manipulation achieved in Rashba rings by introducing weak inplane Zeeman fields.²² (ii) At the degeneracy points ($\phi_d = 0$), the global phase reduces to a purely geometric phase of magnitude $\phi_g = (N-2)\pi$. For an even N , this multiple of 2π corresponds to the geometric phase associated to the solid angle of $N/2 - 1$ full spheres. This means that between consecutive degeneracies the geometric phase undergoes an integer number of windings $w_g = \phi_g/2\pi = N/2 - 1$, which is a topological indicator of the spin dynamics.

The above description differs from what observed in Fig. 2(d) for Rashba rings. There, both the global and dynamic spin phases, ϕ (black) and ϕ_d (blue), grow monotonically with $k_R P$. This growing becomes linear as the spin dynamics turns adiabatic for large $k_R P$. The adiabatic regime is particularly well illustrated by the evolution of the geometric spin phase ϕ_g (red), approaching $-\pi$ for large $k_R P$ as expected for spin states aligned with the radial Rashba field. In this limit, the spin states orbit the equator of the Bloch sphere by subtending a solid angle corresponding to half sphere. Figure 2(d) represents an effective decoupling between dynamic and geometric spin phases in rings, which is absent in polygons due to the emergence of degeneracy points.

We further notice in Fig. 2 that spin phases in polygons mimic the behavior observed in rings in the regime of weak Rashba SOC strengths $k_R P \ll N$, namely, far from first degeneracy point. Deep in that weak-field

limit, Rashba polygons and rings become practically indistinguishable from the point of view of the gathered spin phases.

B. Conductance

Here we show that the spin-phase characteristics discussed in the previous Sec. III A have observable consequences in the conductance of Rashba polygons. To this aim, we consider Rashba polygons with N (even) sides symmetrically coupled to source and drain contact leads as shown in Fig. 1. We adopt the Landauer-Büttiker formulation⁴⁰ at zero temperature by identifying the linear conductance G with the quantum transmission T (in units of the quantum of conductance e^2/h): $G = (e^2/h)T$, with $T = \sum_{mn} |t_{mn}|^2$ and t_{mn} the quantum transmission amplitude from the incoming mode n at the source contact lead to the outgoing mode m at the drain contact lead. In our one-dimensional model we have one single orbital mode and two spin modes, such that $0 \leq T \leq 2$. Moreover, the unitarity of the scattering matrix imposes $T + R = 2$, where $R = \sum_{mn} |r_{mn}|^2$ is the quantum reflection with r_{mn} the corresponding amplitudes for incoming and outgoing modes n and m at the source contact lead.

A realistic modelling of the experimental conditions, as those corresponding to two-dimensional Rashba loop arranges,^{21,22,33} requires to take into account the effect of disorder and/or sample averaging. By following a semi-classical approach for loops strongly coupled to the contact leads (see Appendix A) we distinguish two different situations:

(i) Systems preserving a two-fold reflection symmetry along the axis connecting the contact leads. In this case, the basic traits of the quantum conductance are captured by the expression

$$G_1 = \frac{e^2}{h}(1 + \cos \phi), \quad (6)$$

with ϕ the global spin phase defined in Sec. III A. The resulting pattern, oscillating as a function of $k_R P$ (through ϕ), is the AC interference effect in Rashba loops.^{8,10,11}

(ii) Systems with broken geometrical symmetries. In this case, the quantum conductance is best described by the expression

$$G_2 = \frac{e^2}{h}(1 - \cos 2\phi). \quad (7)$$

Equation (7) captures the pairing of time-reversed orbital path emerging in disordered systems. In the absence of Rashba SOC ($\phi = 0$), this pairing leads to a minimum in the quantum conductance due to the constructive interference of backscattered carriers, an effect known as weak localization. For sufficiently strong Rashba SOC (e.g., $\phi = \pi/2$), this effect is reversed by destructive interference of backscattered spin carriers maximizing the

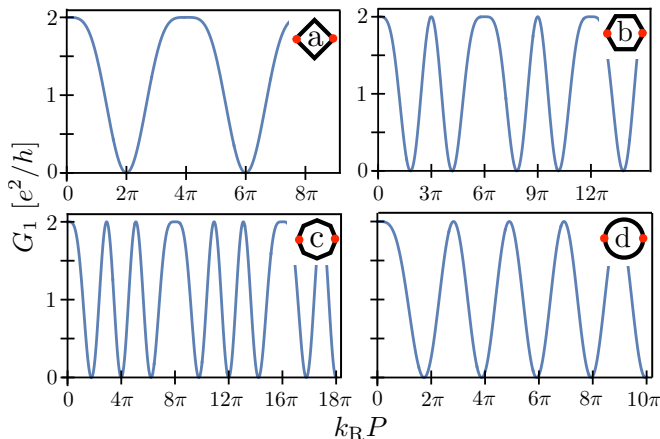


FIG. 4. Conductance G_1 of Eq. (6) as a function of the Rashba coupling strength $k_R P$ corresponding to two-fold symmetric (a) squares, (b) hexagons, (c) octagons, and (d) rings.

quantum conductance, leading to the so-called weak antilocalization. This pattern oscillates with a frequency two times larger than the one observed for G_1 in Eq. (6). This frequency doubling shares its origin with the Al'tshuler-Aronov-Spivak oscillations⁴¹ observed in magnetoconductance experiments with disordered rings and squares.^{21,22,33} Hence, the relevance of either G_1 or G_2 for a given implementation can be decided independently in the laboratories by performing complementary magnetoconductance measurements and observing the periodicity of the oscillations in units of the magnetic flux quantum $\phi_0 = hc/e$.

Figures 4 and 5 illustrate the results of Eqs. (6) and (7), respectively, by plotting G_1 and G_2 as a function of $k_R P$. Two particular features stand out there: (i) The extremes of the global phase ϕ —related to degeneracy points due to vanishing dynamic phases, as shown in Fig. 2—manifest as conductance plateaus. (ii) Away from the degeneracy points, in the regime where the global phase ϕ responds linearly to $k_R P$, the conductance displays rapid AC oscillations dominated by the dynamic spin phase. These features explain the presence of two different frequencies contributing to the AC conductance oscillations in polygons: a lower frequency given by the periodicity of the global phase and a higher frequency determined by large phase-gathering rates between global phase extremes. One consequence is that the lower frequency contribution dominates in squares while it is absent in rings. Such contributing frequencies have been previously identified²⁶ and discussed²⁹ in terms of length scales, i.e., the perimeter P and the segments length $L = P/N$ measured in units of the spin-precession length $L_R = \pi/k_R$. However, the non-monotonicity of the gathered spin phases and the presence of emergent spin degeneracies passed unnoticed in those discussions.

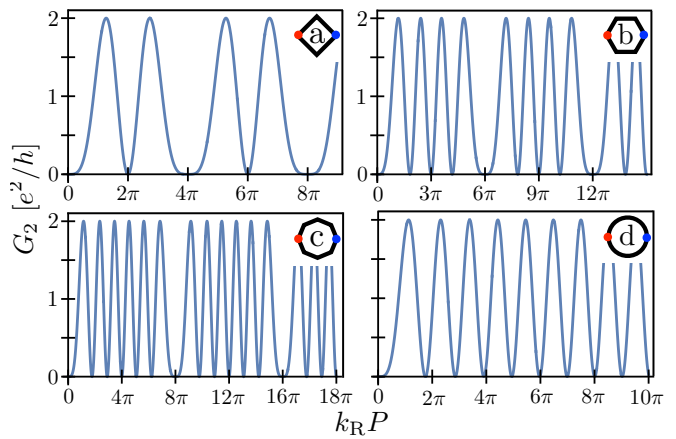


FIG. 5. Conductance G_2 of Eq. (7) as a function of the Rashba coupling strength $k_R P$ corresponding to disordered (a) squares, (b) hexagons, (c) octagons, and (d) rings. Notice the frequency doubling with respect to the results of Fig. 4 due to time-reversed path interference (dual of the magnetoconductance Al'tshuler-Aronov-Spivak oscillations). The minima for $k_R P = 0$ is due to weak localization.

IV. CONCLUSIONS

We have demonstrated that spin carriers propagating in circuits of polygonal shape gather spin phases in a non-monotonic fashion as a function of the Rashba SOC strength. This peculiar behaviour is triggered by the inhomogeneities of the geometric curvature along the polygonal perimeter—where flat segments alternate with highly curved vertices—introducing effective Rashba field discontinuities acting as scattering centers for spin. As a consequence, a periodic series of spin degeneracy points emerge. This contrasts with the case of ring circuits of constant curvature, which present a monotonous phase gathering and a complete absence of spin degeneracies. We find that the global spin phases oscillate with a period determined by the emergent degeneracies. Moreover, dynamic and geometric spin-phase components present a rich pattern allowing the independent control of dynamic phases over geometric-phase plateaus (complementary to previous findings on the independent control of geometric spin phases in Rashba rings²²).

We have also shown that the non-monotonicity of the spin-phase gathering has definite consequences in AC conductance oscillations as the presence of plateaus in the vicinity of spin degeneracies and the participation of two different frequencies. These frequencies were identified in previous works^{26,29} but interpreted in terms of the different length scales present in the system, overlooking the particulars of the spin-phase gathering and the existence of spin degeneracies.

Our findings offer original ways to engineer electronic spin phases at the mesoscopic scale by geometric means. The identification of emergent degeneracies suggest that non-abelian geometric spin phases may also apply. The

role played by commensurability effects in the development of emergent degeneracies and phase gathering remains an open question, motivating future investigations on irregular polygons. The relevance shown by the geometric curvature in the reported findings also suggest that prospective studies of spin dynamics in non-euclidean surfaces are in order.

ACKNOWLEDGMENTS

This work was supported by the Spanish Ministerio de Ciencia, Innovación y Universidades through Project No. FIS2017-86478-P.

Appendix A: Semiclassical conductance

The Landauer-Büttiker formulation⁴⁰ identifies the two-contact linear conductance G with the quantum transmission and reflection as

$$G = \frac{e^2}{h} \text{tr} [\mathbb{T} \mathbb{T}^\dagger] = \frac{e^2}{h} \text{tr} [\mathbb{I} - \mathbb{R} \mathbb{R}^\dagger], \quad (\text{A1})$$

with $\mathbb{T} = [t_{mn}]$ and $\mathbb{R} = [r_{mn}]$, where t_{mn} and r_{mn} are the quantum transmission and reflection amplitudes from incoming (n) to outgoing (m) modes. The trace of \mathbb{I} equals the number of available incoming modes. A semiclassical model⁴² of G for one-dimensional Rashba loops can be developed whenever the carriers wavelength is much smaller than the system size and the spin splitting is much smaller than the kinetic energy (so that the spin dynamics does not alter the orbital one),⁴³ in agreement with mesoscopic experimental conditions.^{21,22,33} In this way, by following a path-integral approach and taking the semiclassical limit,⁴⁴ the quantum transmission and reflection amplitudes can be expressed as

$$t_{mn} = \sum_{\Gamma} a_{\Gamma} e^{ik_{\text{F}} L_{\Gamma}} \langle m | U_{\Gamma} | n \rangle, \quad (\text{A2})$$

$$r_{mn} = \sum_{\Gamma} b_{\Gamma} e^{ik_{\text{F}} L_{\Gamma}} \langle m | U_{\Gamma} | n \rangle, \quad (\text{A3})$$

namely, as a sum of phase contributions over different classical paths Γ of length L_{Γ} taking the spin carriers from entrance to exit leads with different statistical weights a_{Γ} and b_{Γ} , eventually leading to quantum interference. Within this picture, charge and spin contributions are clearly differentiated. The charge contributes with the action phase $\exp[ik_{\text{F}} L_{\Gamma}]$. As for the spin, carriers entering the system with spin n can leave it with spin m according to the path-dependent spin evolution operator U_{Γ} , which is determined by the particular fields experienced by the spin carriers along the classical path. As for the quantum transmission and reflection, they con-

sist of probability terms of the form

$$|t_{mn}|^2 = \sum_{\Gamma, \Gamma'} a_{\Gamma} a_{\Gamma'}^* e^{ik_{\text{F}}(L_{\Gamma} - L_{\Gamma'})} \langle m | U_{\Gamma} | n \rangle \langle m | U_{\Gamma'} | n \rangle^* \quad (\text{A4})$$

$$|r_{mn}|^2 = \sum_{\Gamma, \Gamma'} b_{\Gamma} b_{\Gamma'}^* e^{ik_{\text{F}}(L_{\Gamma} - L_{\Gamma'})} \langle m | U_{\Gamma} | n \rangle \langle m | U_{\Gamma'} | n \rangle^* \quad (\text{A5})$$

For a realistic modelling of the experimental conditions, the effects of disorder and/or sample averaging need to be taken into account. This means that the sums in (A4) and (A5) need to run over different configurations including classical path fluctuations. Moreover, an average over a small energy window around the Fermi energy can be also implemented to take into account the effects of finite (though low) temperatures. Due to the presence of the orbital-phase factors $\exp[ik_{\text{F}}(L_{\Gamma} - L_{\Gamma'})]$, the averaging procedure shows that the only surviving terms in (A4) and (A5) are those corresponding to pairs of paths $\{\Gamma, \Gamma'\}$ with the same geometric length, $L_{\Gamma} = L_{\Gamma'}$. Other contributions simply average out due to rapid oscillations of the orbital-phase factors. However, identifying these pairs of paths contributing to the transmission in (A4) is generally difficult unless two-fold reflection symmetry along the axis connecting the contact leads is preserved. Otherwise, it results most convenient to resort to the quantum reflection (A5) by taking advantage of unitarity. Moreover, when the conducting loops are well coupled to the leads, the carriers tend to escape after a few windings. In this case, it has been shown that the most relevant features of the conductance are fully captured by considering only the shortest paths.^{11,22,33}

By assuming two-fold symmetric configurations and well-coupled leads, the conductance can be calculated from the simplified transmission amplitudes

$$t_{mn} = \frac{1}{2} \langle m | U_+(N/2 + 1) + U_-(N/2 + 1) | n \rangle, \quad (\text{A6})$$

with

$$U_+(N/2 + 1) = R_{N/2+1, N/2} \dots R_{32} R_{21}, \quad (\text{A7})$$

$$U_-(N/2 + 1) = R_{N/2+1, N/2+2} \dots R_{N-1, N} R_{N1}, \quad (\text{A8})$$

and R_{vu} defined in Eq. (2). Notice that we have dropped the phase factor $\exp[ik_{\text{F}} P/2]$ from Eq. (A6) corresponding to CCW/CW orbital paths of length $P/2$, which have turned irrelevant to the transmission. By using time-reversal symmetry ($R_{vu}^\dagger = R_{uv}$) and working in the eigenbasis of $U_{\pm}(N)$, Eq. (5), we find from Eq. (A1) that the conductance within this approximation takes the form⁴⁵

$$G_1 = \frac{e^2}{h} (1 + \cos \phi),$$

with ϕ the global spin phase gathered by the carriers in a round trip.

However, in most experimental situations the two-fold symmetry can not be assumed. This general case can be modelled by resorting to the reflection probabilities

(A5) after noticing that, for any backscattering path Γ , there exists another path $\tilde{\Gamma}$ with exactly the same length that follows the trajectory defined by Γ but in opposite direction. Namely, Γ and $\tilde{\Gamma}$ are time-reversed paths. By considering well-coupled leads, we find that they correspond to CCW/CW single-winding paths of length P . The corresponding reflection amplitudes take the form

$$r_{mn} = \frac{1}{2} \langle m | U_+(N) + U_-(N) | n \rangle, \quad (\text{A9})$$

where we have dropped the irrelevant phase factor $\exp[ik_F P]$. By turning to time-reversal symmetry and the eigenbasis of $U_{\pm}(N)$, in this case we find a conductance⁴⁵

$$G_2 = \frac{e^2}{h} (1 - \cos 2\phi),$$

where the minus sign and the factor 2 in the argument are the consequences of the time-reversed path pairing.

-
- * frustaglia@us.es
- ¹ A. Hirohata, K. Yamada, Y. Nakatani, I.-L. Prejbeanu, B. Diény, P. Pirro, and B. Hillebrands, Review on spintronics: Principles and device applications, *J. Magn. Magn. Mater.* 509, 166711 (2020).
 - ² G. Bergmann, Weak anti-localization— An experimental proof for the destructive interference of rotated spin 1/2, *Solid State Commun.* 42, 815 (1982).
 - ³ F.E. Meijer, A.F. Morpurgo, T.M. Klapwijk, and J. Nitta, Universal Spin-Induced Time Reversal Symmetry Breaking in Two-Dimensional Electron Gases with Rashba Spin-Orbit Interaction, *Phys. Rev. Lett.* 94, 186805 (2005).
 - ⁴ S. Datta and B. Das, Electronic analog of the electro-optic modulator, *Appl. Phys. Lett.* 56, 665 (1990).
 - ⁵ F. Mireles and G. Kirczenow, Ballistic spin-polarized transport and Rashba spin precession in semiconductor nanowires, *Phys. Rev. B* 64, 024426 (2001).
 - ⁶ H.C. Koo, J.H. Kwon, J. Eom, J. Chang, S.H. Han, and M. Johnson, Control of Spin Precession in a Spin-Injected Field Effect Transistor, *Science* 325, 1515 (2009).
 - ⁷ P. Chuang, S.-C. Ho, L.W. Smith, F. Sfigakis, M. Pepper, C.-H. Chen, J.-C. Fan, J.P. Griffiths, I. Farrer, H.E. Beere, G.A.C. Jones, D.A. Ritchie, and T.-M. Chen, All-electric all-semiconductor spin field-effect transistors, *Nat. Nanotechnol.* 10, 35 (2015).
 - ⁸ Y. Aharonov and A. Casher, Topological Quantum Effects for Neutral Particles, *Phys. Rev. Lett.* 53, 319 (1984).
 - ⁹ H. Mathur and A.D. Stone, Quantum transport and the electronic Aharonov-Casher effect, *Phys. Rev. Lett.* 68, 2964 (1992).
 - ¹⁰ J. Nitta, F. E. Meijer, and H. Takayanagi, Spin-interference device *Appl. Phys. Lett.* 75, 695 (1999).
 - ¹¹ D. Frustaglia and K. Richter, Spin interference effects in ring conductors subject to Rashba coupling, *Phys. Rev. B* 69, 235310 (2004).
 - ¹² T. Bergsten, T. Kobayashi, Y. Sekine, and J. Nitta, Experimental Demonstration of the Time Reversal Aharonov-Casher Effect, *Phys. Rev. Lett.* 97, 196803 (2006).
 - ¹³ M. König, A. Tschetschetkin, E.M. Hankiewicz, J. Sinova, V. Hock, V. Daumer, M. Schäfer, C.R. Becker, H. Buhmann, and L.W. Molenkamp, Direct Observation of the Aharonov-Casher Phase, *Phys. Rev. Lett.* 96, 076804 (2006).
 - ¹⁴ B. Grbić, R. Leturcq, T. Ihn, K. Ensslin, D. Reuter, and A.D. Wieck, Aharonov-Bohm Oscillations in the Presence of Strong Spin-Orbit Interactions, *Phys. Rev. Lett.* 99, 176803 (2007).
 - ¹⁵ A. Manchon, H.C. Koo, J. Nitta, S. M. Frolov, and R. A. Duine, New perspectives for Rashba spin-orbit coupling, *Nat. Mater.* 14, 871 (2015).
 - ¹⁶ D. Bercioux and P. Lucignano, Quantum transport in Rashba spin-orbit materials: a review, *Rep. Prog. Phys.* 78, 106001 (2015).
 - ¹⁷ V. Mourik, K. Zuo, S.M. Frolov, S.R. Plissard, E.P.A.M. Bakkers, and L.P. Kouwenhoven, Signatures of Majorana Fermions in Hybrid Superconductor-Semiconductor Nanowire Devices, *Science* 336, 1003 (2012).
 - ¹⁸ Y.A. Bychkov and E.I. Rashba, Oscillatory effects and the magnetic susceptibility of carriers in inversion layers, *J. Phys. C* 17, 6039 (1984).
 - ¹⁹ J. Nitta, T. Akazaki, H. Takayanagi, and T. Enoki, Gate control of spin-orbit interaction in an inverted InGaAs/InAlAs heterostructure, *Phys. Rev. Lett.* 78, 1335 (1997).
 - ²⁰ Y. Aharonov and D. Bohm, Significance of Electromagnetic Potentials in the Quantum Theory, *Phys. Rev.* 115, 485 (1959).
 - ²¹ F. Nagasawa, J. Takagi, Y. Kunihashi, M. Kohda, and J. Nitta, Experimental Demonstration of Spin Geometric Phase: Radius Dependence of Time-Reversal Aharonov-Casher Oscillations, *Phys. Rev. Lett.* 108, 086801 (2012).
 - ²² F. Nagasawa, D. Frustaglia, H. Saarikoski, K. Richter, and J. Nitta, *Nature Comm.* 4, 2526 (2013).
 - ²³ H. Saarikoski, A. Reynoso, J.P. Baltanás, D. Frustaglia, and J. Nitta, Spin interferometry in anisotropic spin-orbit fields, *Phys. Rev. B* 97, 125423 (2018).
 - ²⁴ F. Nagasawa, A.A. Reynoso, J.P. Baltanás, D. Frustaglia, H. Saarikoski, and J. Nitta, Gate-controlled anisotropy in Aharonov-Casher spin interference: Signatures of Dresselhaus spin-orbit inversion and spin phases, *Phys. Rev. B* 98, 245301 (2018).
 - ²⁵ D. Frustaglia and J. Nitta, Geometric spin phases in Aharonov-Casher interference, *Solid State Commun.* 311, 113864 (2020).
 - ²⁶ D. Bercioux, D. Frustaglia, and M. Governale, Signatures of spin-related phases in transport through regular polygons, *Phys. Rev. B* 72, 113310 (2005).
 - ²⁷ T. Koga, Y. Sekine, and J. Nitta, Experimental realization of a ballistic spin interferometer based on the Rashba effect using a nanolithographically defined square loop array, *Phys. Rev. B* 74, 041302(R) (2006).
 - ²⁸ F. Qu, F. Yang, J. Chen, J. Shen, Y. Ding, J. Lu, Y. Song, H. Yang, G. Liu, J. Fan, Y. Li, Z. Ji, C. Yang, and L. Lu, Aharonov-Casher Effect in Bi2Se3 Square-Ring Interferometers, *Phys. Rev. Lett.* 107, 016802 (2011).
 - ²⁹ A. Hijano, T. L. van den Berg, D. Frustaglia, and D. Bercioux, Quantum network approach to spin interferometry driven by Abelian and non-Abelian fields, *Phys. Rev.*

- B 103, 155419 (2021).
- ³⁰ C. Ortix, Quantum mechanics of a spin-orbit coupled electron constrained to a space curve, Phys. Rev. B 91, 245412 (2015).
- ³¹ Z.-J. Ying, P. Gentile, C. Ortix, and M. Cuoco, Designing electron spin textures and spin interferometers by shape deformations, Phys. Rev. B 94, 081406(R) (2016).
- ³² Z.-J. Ying, P. Gentile, J.P. Baltanás, D. Frustaglia, C. Ortix, and M. Cuoco, Geometric driving of two-level quantum systems, Phys. Rev. Research 2, 023167 (2020).
- ³³ M. Wang, H. Saarikoski, A.A. Reynoso, J.P. Baltanás, D. Frustaglia, and J. Nitta, Geometry-Assisted Topological Transitions in Spin Interferometry, Phys. Rev. Lett. 123, 266804 (2019).
- ³⁴ T. Salamone, M.B.M. Svendsen, M. Amundsen, and S. Jacobsen, Curvature-induced long ranged supercurrents in diffusive SFS Josephson Junctions, with dynamic $0 - \pi$ transition, arXiv:2105.13372.
- ³⁵ M. Popp, D. Frustaglia, and K. Richter, Conditions for adiabatic spin transport in disordered systems, Phys. Rev. B 68, 041303(R) (2003).
- ³⁶ D. Loss, P. Goldbart, and A.V. Balatsky, Berry's phase and persistent charge and spin currents in textured mesoscopic rings, Phys. Rev. Lett. 65, 1655 (1990).
- ³⁷ A. Stern, Berry's phase, motive forces, and mesoscopic conductivity, Phys. Rev. Lett. 68, 1022 (1992).
- ³⁸ A.G. Aronov and Y.B. Lyanda-Geller, Spin-Orbit Berry Phase in Conducting Rings, Phys. Rev. Lett. 70, 343 (1993).
- ³⁹ Y. Aharonov and J. Anandan, Phase change during a cyclic quantum evolution, Phys. Rev. Lett. 58, 1593 (1987).
- ⁴⁰ M. Büttiker, Y. Imry, R. Landauer, and S. Pinhas, Generalized many-channel conductance formula with application to small rings, Phys. Rev. B 31, 6207 (1985).
- ⁴¹ B. L. Al'tshuler, A. G. Aronov, and B. Z. Spivak, The Aharonov-Bohm effect in disordered conductors, JETP Lett. 33, 94 (1981).
- ⁴² For reviews on semiclassical theory, see e.g. K. Richter, *Semiclassical Theory of Mesoscopic Quantum Systems* (Springer, Berlin, 2000); R.A. Jalabert, in *New Directions in Quantum Chaos*, G. Casati, I. Guarneri, and U. Smilansky, eds. (IOS Press, Amsterdam, 2000).
- ⁴³ H. Frisk and T. Guhr, Spin-Orbit Coupling in Semiclassical Approximation, Ann. Phys. (N.Y.) 221, 229 (1993).
- ⁴⁴ D. Loss and P. Goldbart, Persistent currents from Berry's phase in mesoscopic systems, Phys. Rev. B 45, 13544 (1992).
- ⁴⁵ By using the properties of the trace we find that

$$\text{tr} [\mathbb{T}\mathbb{T}^\dagger] = \frac{1}{2} \text{tr} \left[\mathbb{I} + \begin{pmatrix} e^{i\phi} & 0 \\ 0 & e^{-i\phi} \end{pmatrix} \right] = 1 + \cos \phi,$$

with

$$\mathbb{T} = \frac{1}{2} [U_+(N/2 + 1) + U_-(N/2 + 1)].$$

Similarly, we find

$$\text{tr} [\mathbb{R}\mathbb{R}^\dagger] = \frac{1}{2} \text{tr} \left[\mathbb{I} + \begin{pmatrix} e^{i2\phi} & 0 \\ 0 & e^{-i2\phi} \end{pmatrix} \right] = 1 + \cos 2\phi,$$

with

$$\mathbb{R} = \frac{1}{2} [U_+(N) + U_-(N)].$$